Universidad de Santiago de Compostela

Study of the shadow of the Sun with a high resolution cosmic ray detector

Jorge Otero Santos

jorge.otero.santos@rai.usc.es

supervised by

Juan Antonio Garzón Heydt

Abstract

English

Cosmic rays are a type of radiation coming from the space that reaches the Earth constantly. These rays and the cascades of particles generated when they reach the atmosphere can be studied with a detector from the surface. A common study in all cosmic ray laboratories all over the world is the study of the shadow of the Sun, a minimum in the cosmic radiation intensity in the direction of the Sun due to the magnetic field, that deflects the particles, changing their trajectories. This study can be a quality test of the detector. This project will run an analysis of the shadow of the Sun using the TRAGALDABAS detector, located at the Faculty of Physics of the Universidad de Santiago de Compostela, to study its angular resolution in the reconstruction of the measured cosmic ray fronts. Making use of the data analysis done, the can also be developed another studies about other related phenomena, like Forbush Decrease.

Castellano

Los rayos cósmicos son un tipo de radiación proveniente del espacio que alcanza la Tierra de forma constante. Estos rayos y las cascadas de partículas a las que dan lugar al alcanzar la atmósfera pueden estudiarse con un detector desde la superficie. Un estudio común en todos los laboratorios de rayos cósmicos del mundo es el estudio de la sombra del Sol, un mínimo en la intensidad de la radiación cósmica en la dirección del Sol debido a que su campo magnético deflecta las partículas, desviando su trayectoria. Este estudio puede servir como test de calidad del detector. En este trabajo de llevará a cabo un análisis de la sombra del Sol utilizando el detector TRAGALDABAS situado en la Facultad de Física de la Universidad de Santiago de Compostela para estudiar su resolución angular en la recostrucción de los frentes de rayos cósmicos medidos. Mediante el análisis de datos realizado también pueden llevarse a cabo estudios de otros fenómenos relacionados relacionados, como el Forbush Decrease.

Galego

Os raios cósmicos son un tipo de radiación provinte do espacio que alcanza a Terra de forma constante. Estes raios e as cascadas de partículas ás que dan lugar ó alcanzar a atmosfera poden estudarse cun detector desde a superficie. Un estudo común en tódolos laboratorios de raios cósmicos do mundo é o estudo da sombra do Sol, un mínimo de intensidade da radiación cósmica na dirección do Sol debido a que o seu campo magnético deflecta as partículas, cambiando a súa traxectoria. Este estudo pode servir como test de calidade do detector. Neste traballo levarase a cabo unha análise da sombra do Sol utilizando o detector TRAGALDABAS situado na Facultade de Física de Santiago de Compostela para estudar a súa resolución angular na reconstrución dos frentes de raios cósmicos medidos. Mediante a análise de datos realizada tamén poden levarse a cabo estudos de outros fenómenos relacionados, como o Forbush Decrease.

Contents

1 Introducction **3**

1.1 Cosmic rays 3

1.2 Shadow of the Sun 4

2 The TRAGALDABAS detector **5**

3 Coordinate systems **7**

3.1 Coordinate transformations 9

3.2 First test: Transformation of a uniform distribution 12

3.3 Generation of Sun's coordinates 13

4 Data analisys **14**

4.1 Data sample 14

4.2 Acceptance corrections 14

4.3 Shadow of the Sun 15

4.4 Forbush Decrease 18

5 Conclusions **23**

1 Introducction

1.1 Cosmic rays

Cosmic rays is the name given to the subatomic particles that reach the Earth's atmosphere every second coming from deep space with a high degree of isotropy. They are composed mainly by protons, some light nuclei (arround 25% are alpha particles and 13% carbon, oxygen or nitrogen nuclei), electrons and gamma rays. Cosmic rays that reach the Earth cover a wide range of energies.

Low energy cosmic rays are very common and they come mostly from sources close to Earth, like the Sun. These low energy cosmic rays are deflected due to the interaction with the atmosphere and the Earth's magnetic field. As the energy increases, the frecuency and the flux decrease, and the particles are less affected by the magnetic field and they are able to penetrate deeper in the atmosphere. This is shown in figure 1:

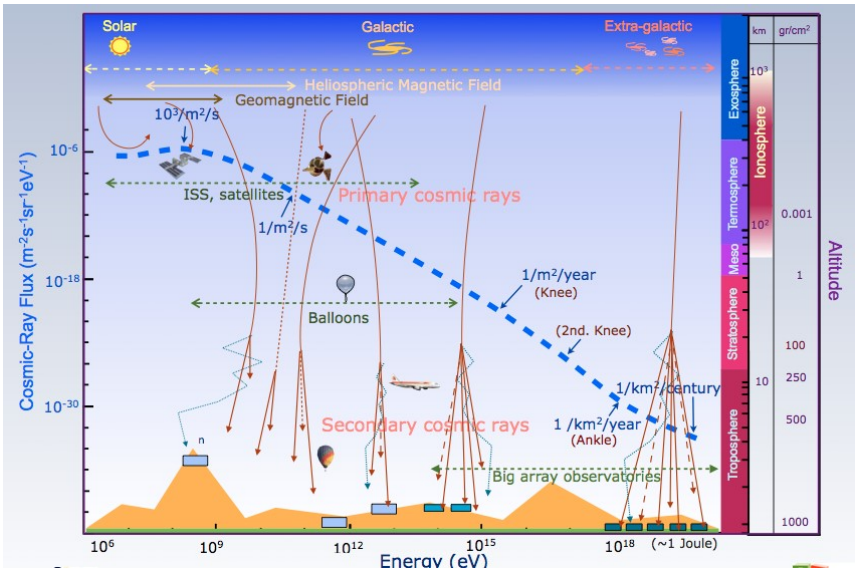

Figure 1: Flux of the cosmic rays as a funtion of the energy

Particles around the zone called "knee", which can be seen in the figure 1, are known as very high energy cosmic rays. Cosmic rays within this energy range hit the atmosphere with a frequency around 1 particle/cm$^2 \cdot s$.

When the high energy cosmic rays reach the atmosphere, they produce a cascade of subatomic particles. At the upper atmosphere, the particles collide with nuclei in the air, resulting in a reaction that causes the release of multiple particles. These new particles cause a secondary wave of interactions, continuing the cascad,e that spreads out producing over one billion of secondary particles. The shower can spread up to several km^2. As there is not always possible to cover such big area, an alternative to use a big array of detectors is to use small detectors measuring a limited sample of the secondary particles created during the shower.

There are three main components of this cosmic ray showers: the mesonic component, the electromagnetic component and the hadronic component.

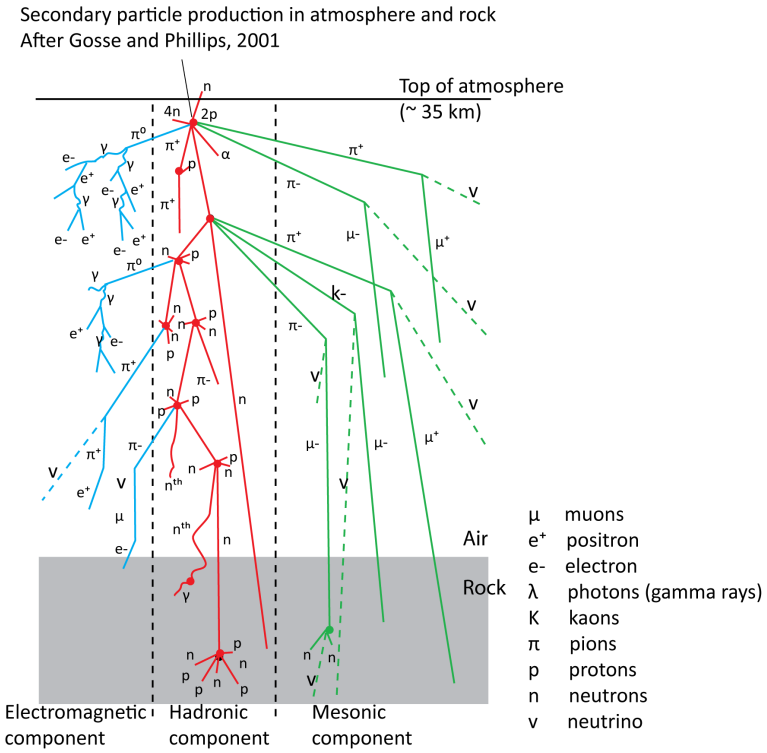

Figure 2: Different components of a cosmic ray cascade

For the highest energy cosmic rays (above 10^{16} eV), the frequency falls to aproximately 1 particle/km^2· century. This is the region called the "ankle".

1.2 Shadow of the Sun

Low energy cosmic rays come mostly from nearby sources, meanwhile, high energy cosmic rays come from the deep space. As it was explained before, this low energy radiation interacts with the Earth's magnetic field, causing the deflection of the incoming particles, avoiding them to reach the Earth. On the other hand, high energy cosmic rays have energy enough to reach the Earth despite the interaction with the magnetic field.

This is why, when a cosmic ray detector points to the Sun, it will register a minimum in the frequency and the number of high energy cosmic rays in that direction. The Sun releases mainly low energy cosmic rays, that will be deflected, so a detector will register a low number of events. This region with low frequency corresponds to the cosmic ray Sun shadow.

The study of this phenomenon is a key factor in the calibration of a big cosmic ray observatory, commonly made at all observatories as a quality test, in order to determinate the angular resolution of the detector. It is usually complemented with the study of the cosmic ray Moon shadow.

Although our detector has a limited resolution and there is the posibility of not seeing the shadow of the Sun because of this present limited resolution, it's important to do all the data analysis and develop the algorithms and test the analysis programs to use them when the detector is improved.

At figure 3 is represented as an example one of the results of the study of the shadow of the Sun with the Milagro detector located at Los Alamos, New Mexico [6][8].

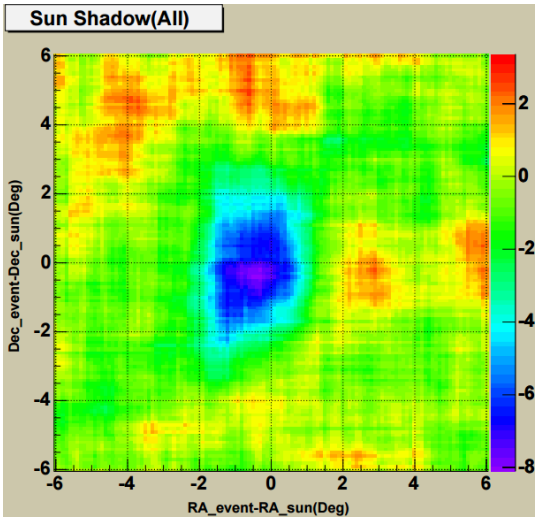

Figure 3: Example of the results obtained at Milagro observatory of the shadow of the Sun

2 The TRAGALDABAS detector

The TRAGALDABAS detector [1] is the first prototype of the TRASGO concept, a new family of high-performance tracking detectors for the study of cosmic rays. It is installed in the Lab 106 of the Faculty of Physics of the University of Santiago de Compostela (USC). Being installed in the first floor of a two-floor building can slightly affect the lowest energy EM components os the cosmic ray's cascades, but this is not very relevant for most of the studies. It is based on the timing RPC technology offering high granularity and high time resolution, with tracking capability.

The detector is composed by four RPC planes, each of them with a surface of 1.2x1.5 m^2, divided in 120 cells with a dimension of 11.1x11.6 cm^2, with a time resolution of aproximately 340 ps. This arrangement allows to reconstruct tracks with a time resolution better than 200 ps and a track angular resolution slightly better than 2^o, that will be improved in the future to below 0.5^o. The angular resolution of cosmic ray showers will be slightly lower. Figure 4 shows the external layout of the detector.

Planes are placed at heights of 0, 90, 120 and 180 cm, in order to cover different angular acceptances. This RPC planes were built at LIP-Coimbra with the same technology that is being tested in the P. Auger observatory in Argentina. Each plane is made by 3 slides of 2 mm wide glasses with a 1 mm gap in between, and placed inside a metacrilate box. In order to compensate the gas losses, a small flux of R134a type freon is constantly flowing. The external sides of the external glass plates are covered by a conductive coating, with a voltage of $\pm$5600 V. The read-out is made by the 120 pads, made by Cu, located at the outer side of the metacrilate

[1] Acronym for "TRAsGo for the AnaLisys of the nuclear matter Decay, the Atmosphere, the earth B-Field And the Solar activity".

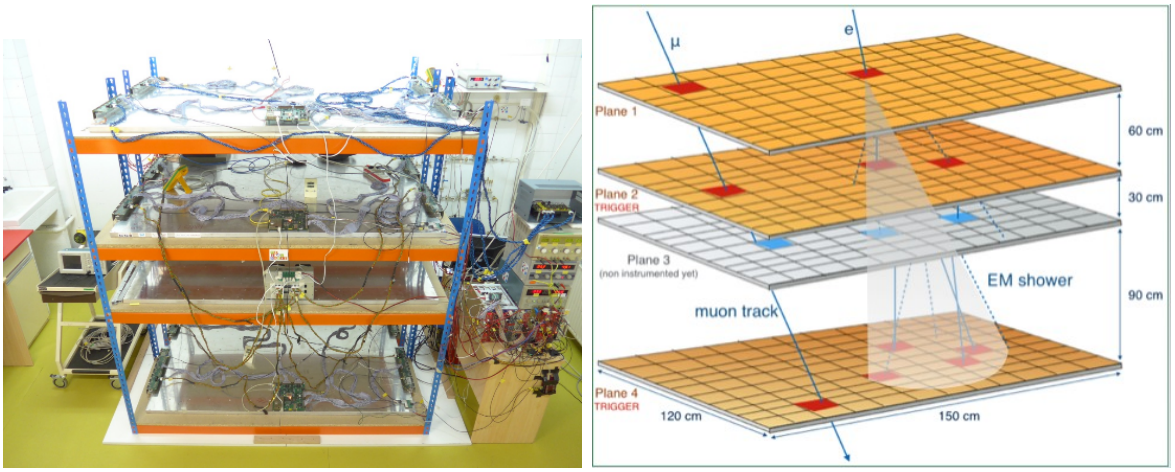

(a) Detector's external layout (b) Track recontruction

Figure 4: Images of the TRAGALDABAS detector and its reconstruction capabilities

box, at 10 mm distance of each other. This cells are separated by straight guard-electrodes 6 mm wide to prevent the crosstalk, that is almost negligible. [2]

TRAGALDABAS uses the same read-out front end electronics (FEE) that is being succesfully used by the HADES nuclear physics experiment, at the GSI, located at Darmstadt, Germany. This type off FEE is based on a motherboard (MB) - daughterboard (DB) philosophy. The RPC signals are first aplified and integrated, and then digitalized in a single board in LVDS format in the 4-channel DB's. The leading edge of the signal gives the arrival time of the particle, in the width of the signal, the induced charge is codified by a "charge to width" (QtoW) method. Each MB has eight DB's, giving them the low voltage and the output fot both the digital read-out and the trigger signals. [3]

The detector also counts with a slow control system based on a NAGIOS service, supervising the high voltage operation currents, pressure, humidity and temperature, building an I2C bus conected to a Rasberry Pi for the monitoring of this magnitudes.

In addition, the detector is equipped with a reconstruction software done within a specific framework based on ROOT and written in C++. This data analysis reconstructs the events sequentially, unpacking and converting the recorded data to physic units following tables, and calibrating the flight time. The hits are combined into track candidates and finally combined in order to define an arrival direction of the shower.

The detector is taking data every day, with a rate of about 7 millions of registered events per day. 60% of this events correspond to multiplicity M=1, 22% to M=2 and aproximately a 4% correspond to $M \geq 2$. This data is compacted and sent to the supercomputing center (CESGA) fot their definitive storage and handling.

Until July 2016 there where only two active planes (planes 2 and 4). The detector registers an event when there is a coincidence between this two planes. M1 events have one active cell in each plane, M2 have two active cells and M3 more than two cells. Each type of event has also one, two or more than two traces compatible with light speed.

3 Coordinate systems

Local coordinates:

In order to make the data analisys we need our data in a useful coordinate system. The detector gives us information in his local coordinate system, which can be characterized by the angle between the geographic north and the detector's north, and the zenith angle, as we can see in the figure 5:

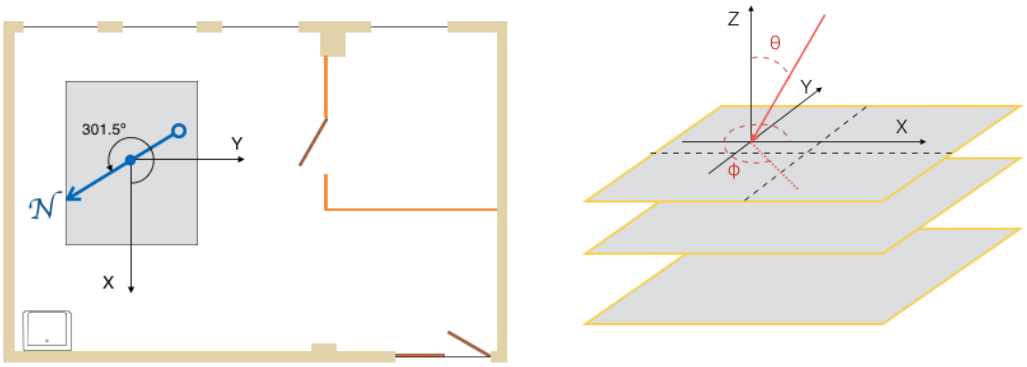

(a) Detector's room arrangement (b) Local reference system

Figure 5: Local coordinates, characterized by z and ϕ

The angles that define the position of a celestial object in this system are the Zenith angle (z), $0^o < z < 180^o$, and the Local azimuth (ϕ), $0^o < \phi < 360^o$.

Our objective is to study the Sun, so this system of coordinates is not very useful as the Sun is moving during all the period of data acquisition, so we will need to refer our data to an alternative celestial coordinate system in which the Sun is a fixed point. To do this, we will use some coordinate transformations.

Horizontal coordinates:

The first step is to change our system into horizontal coordinates. This system uses the observer's local horizon as a fundamental plane, characterizing an object by two coordinates called Altitude (h), $-90^o < h < 90^o$, and Azimuth (A), $0^o < A < 360^o$, as we can see in the figure 6:

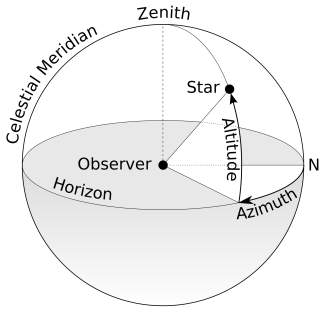

Figure 6: Horizontal coordinates, characterized by the angles A and h

This is a local coordinate system, this means that depending on the position of the observer, the coordinates of the object will change, so we need another transformation to reach a universal coordinate system.

Horary equatorial coordinates:

This system uses as reference the celestial equator, and gives the position of a celestial object with the following two angles: Horary angle (H), $0^o < H < 360^o$, and Declination (δ), $-90^o < \delta < 90$. This is shown in the figure 7:

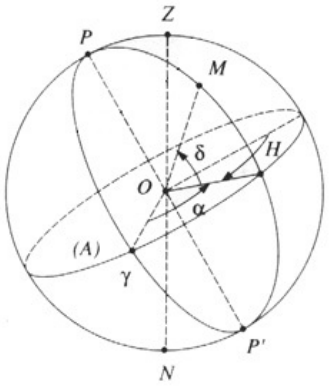

Figure 7: Horary equatorial coordinates, characterized by the angles H and δ

Even though the declination angle is the same for any observer, this coordinate system is still not universal, as the hour angle changes depending on the position of the observer on Earth, so the coordinate system is not universal yet.

Absolute equatorial coordinates:

The absolute equatorial coordinates are defined similarly to the horary equatorial coordinates, the Declination (δ), $-90^o < \delta < 90$, is the same fot both systems because it is a universal coordinate. The other coordinate used is the Right ascension (α), $0^o < \alpha < 360^o$. This is the angle between the vernal equinox or vernal point (γ) and the object's hour circle eastwards. This angles can be seen in the figure 8:

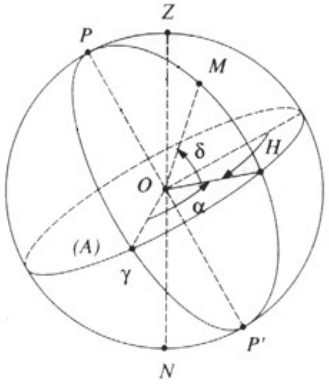

Figure 8: Absolute equatorial coordinates, characterized by the angles α and δ

As the Right ascension is refered to a fixed point, in this system the coordinates of an object are the same regardless of the observer's position. Then, this coordinate system is universal and can be useful for some studies.

Ecliptical coordinates:

The ecliptical coordinate system is commonly used to represent the positions and orbits of Solar System objects. It has as reference plane the ecliptic, the plane that contains the Earth's movement around the Sun. The coordinates that define the position of an object are the Ecliptic longitude (λ), $0^o < \lambda < 360^o$, and the Ecliptic latitude (β), $-90^o < \beta < 90^o$. As it happened with the Right ascension in the absolute ecuatorial coordinates, the origin for the Ecliptic longitude is taken at the vernal point (γ). The origin of the Ecliptic latitude is taken on the ecliptic plane. This is a universal coordinate system.

In our case, we will study the Sun, which is always on the ecliptic, then, the Ecliptic latitude will always be 0^o.

At figure 9 we can see a representation of this coordinate system:

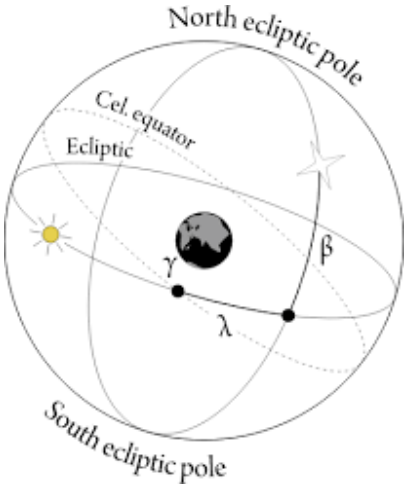

Figure 9: Ecliptic coordinates

Heliocentric coordinates:

The last coordinate system used is the heliocentric coordinate system, which is the same as the ecliptical coordinate system taking the Sun as origin.

3.1 Coordinate transformations

In order to transform one coordinate system into another, we need to define the coordinate transformations [12].

Detector coordinates to Horizontal coordinates:

The transformation between this systems is a rotation of the axes. This is because both systems are the same except for the origin of the azimuthal coordinate. Then:

$$\phi = A + 301.5^o \tag{1}$$

We will also work with the Altitude instead of doing it with the Zenith angle, so the transformation between this two angles is:

$$h = \frac{\pi}{2} - z \tag{2}$$

Horizontal coordinates to Horary equatorial coordinates:

If we know A, h and the observer's latitude (ψ), we can express the relation between these two coordinate systems by Eq.3 and Eq.4:

$$\delta = \sin^{-1}(\sin\psi \sin h + \cos\psi \cos h \cos A) \tag{3}$$

$$H = cos^{-1}\left(\frac{\sin h - \sin\delta \sin\psi}{\cos\delta \cos\psi}\right) \tag{4}$$

with the following condition:

When A<180 then H=H-360

and A>180 then H=H

For the inverse transformations we get the equations 5 and 6:

$$h = \sin^{-1}(\sin\delta \sin\psi + \cos\delta \cos\psi \cos H) \tag{5}$$

$$A = cos^{-1}\left(\frac{\sin\delta - \sin\psi \sin h}{\cos\psi \cos h}\right) \tag{6}$$

with the following angle reduction condition:

If H<180 then A=360-A

If H>180 then A=A

Horary equatorial coordinates to Absolute equatorial coordinates:

This coordinate systems only differ in the the Right ascension, that can be defined from the Hour angle as it follows:

$$\alpha = LST - H \tag{7}$$

The term LST at Eq.7 is the Local sidereal time, knowing as sidereal day the time it takes to Earth to make a complete rotation around herself. Due to the translation movement of the Earth, a sidereal day has not a duration of 24 hours but 23h 56min. The local sidereal time is different depending on the observer's longitude on Earth.

Absolute equatorial coordinates to Ecliptical coordinates:

As we did with absolute and horary equatorial coordinates, we are going to see now the transformation from absolute equatorial coordinates to ecliptical coordinates, given by Eq.8 and Eq.9:

$$\beta = \arcsin(\sin\delta\cos\epsilon - \cos\delta\sin\epsilon\sin\alpha) \tag{8}$$

$$\lambda = \arctan\left(\frac{\sin\delta\sin\epsilon - \cos\delta\cos\epsilon\sin\alpha}{\cos\alpha\cos\delta}\right) \tag{9}$$

If we call "p" to the top part of Eq.9 and "q" to the bottom part, δ follows the next rule:

$$\begin{gathered}\text{If } p\cdot q < 0 \text{ and } q < 0 \text{ then } \lambda = \lambda + 180\\ \text{If } p\cdot q < 0 \text{ and } q > 0 \text{ then } \lambda = \lambda + 360\\ \text{If } p + q < 0 \text{ then } \lambda = \lambda + 180\end{gathered} \tag{10}$$

The parameter $\epsilon = 23.439^o$ written in Eq.8 and Eq.9 represents the obliquity, the angle between the ecliptic and the equator.

The inverse transformation between this two coordinate systems follow equations Eq.11 and Eq.12:

$$\delta = \arcsin(\sin\beta\cos\epsilon - \cos\beta\sin\epsilon\sin\lambda) \tag{11}$$

$$\alpha = \arctan\left(\frac{-\sin\beta\sin\epsilon - \cos\beta\cos\epsilon\sin\lambda}{\cos\lambda\cos\beta}\right) \tag{12}$$

The rule given by Eq.10 is applied to α in the same way as before.

Ecliptical coordinates to Heliocentric coordinates:

Finally we have the transformation from Ecliptical coordinates to Heliocentric coordinates, a system centered at the Sun. The Ecliptic latitude is the same in both cases, it only changes the longitude coordinate. We are not interested in the inverse transformation, so the relation between these two systems is given by Eq.13:

$$\lambda_{heliocentric} = \lambda - \lambda_{Sun} \tag{13}$$

At Eq.13, λ_{Sun} is the Ecliptic longitude of the Sun. We will see how to obtain its value at 3.3. By using this coordinate transformation we obtain a universal coordinate system centered at the Sun.

3.2 First test: Transformation of a uniform distribution

Before making the data analysis we have written and tested these coordinate changes. We used Python, that is one of the standard languages of the TRAGALDABAS collaboration.

Before using the program on our data, we have to check that the transformations have been applied correctly. To make this, a simple first test is using the program on a uniform cosmic ray distribution. This was made by generating a uniform distribution on $\cos\theta \in (-1, 1)$ and $\varphi \in (0, 2\pi)$.

When we apply the transformations to this random and uniform distribution, we should obtain again a uniform distribution in the new coordinate system. Then, using the coordinates transformations on a uniform distribution is the first proof that the program is working right.

The results obtained can be seen at figure 10:

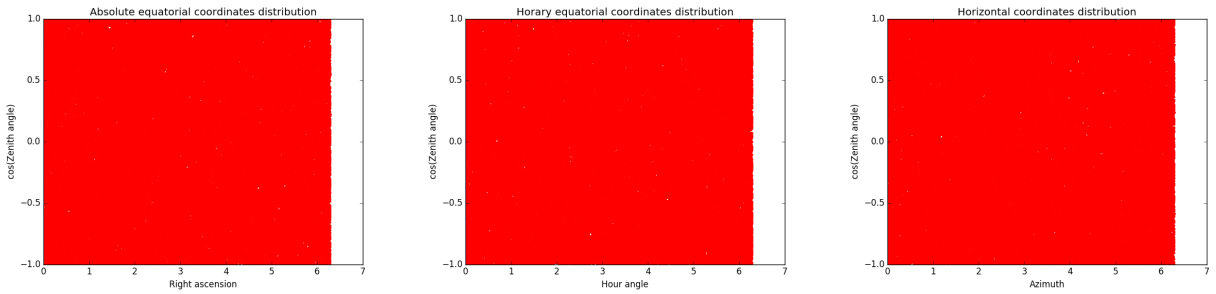

(a) Uniform distribution in absolute equatorial coordinates

(b) Uniform distribution in horary equatorial coordinates

(c) Uniform distribution in horizontal coordinates

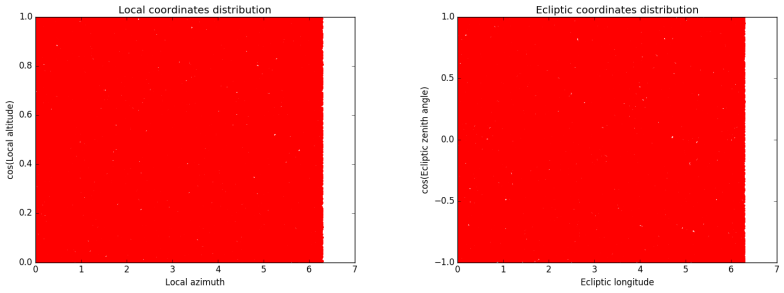

(d) Uniform distribution in local coordinates

(e) Uniform distribution in ecliptic coordinates

Figure 10: Uniform distribution in different coordinate systems

We can see that the cosmic ray distribution remains uniform in all the coordinates systems. If we make the inverse transformations, they should also remain uniform.

3.3 Generation of Sun's coordinates

The next step to check the coordinate transformations is to generate the coordinates os the Sun. This is also needed too to apply the transformation from ecliptic coordinates to heliocentric coordinates.

The ecliptic latitude of the Sun is 0^o as we saw before, and the ecliptic longitude is given by Eq.14 [2]:

$$\lambda_{Sun} = L + 1.915^o \sin g + 0.020^o \sin 2g \tag{14}$$

with

$$L = 280.460^o + 0.9856474^o n$$
$$g = 357.528^o + 0.9856003^o n$$
$$n = JD - 2451545.0$$

In this equation, JD is the Julian Day, which is the number of days and fraction elapsed since 12:00 PM of January 1 of the year 4713 b.C.. In astronomy, is usually taken as reference the Julian date of January 1 of 2000.

We also need the Julian date to get the local sidereal time [3].

With the position of the Sun we can also check if the coordinate transformations are correct, by calculating this positions in the other coordinate systems. If we represent the position if the Sun in absolute equatorial coordinates, given by Eq.15, we obtain the curve shown in the figure 11.a.

$$\begin{aligned} \alpha_{Sun} &= \arctan(\cos\epsilon \tan\lambda_{Sun}) \\ \delta_{Sun} &= \arcsin(\sin\epsilon \sin\lambda_{Sun}) \end{aligned} \tag{15}$$

Also if we take the position of the Sun every day of the year at the same hour, we get the curve at 11.b. This curve is known as the analemma. With our program we see that we can simulate the analemma properly.

Finally, we can represent the same curves, but instead of taking the Sun as point-like, considering it as an extense body, obtaining the same results, and concluding that the program works properly.

[2] Algorithm for the generation of the coordinates of the Sun, more deeply explained at [7].

[3] The local sidereal time is obtained using the expression $LST = GST_t + \psi^o/15$, where ψ is the latitude of the observer and GST_t is the Greenwich sidereal time at any universal time, obtained with the expression $GST_t = GST_0 + UT * 1.0027379$. GST_0 is the Greenwich sidereal time at universal time $UT = 0h$. UT is obtained from the local time (LT) of the observer by applying the correction due to the time zone (TZ) with $UT = LT - TZ$. Time zone is taken positive eastwards and negative westwards. The detailed information is given at [13].

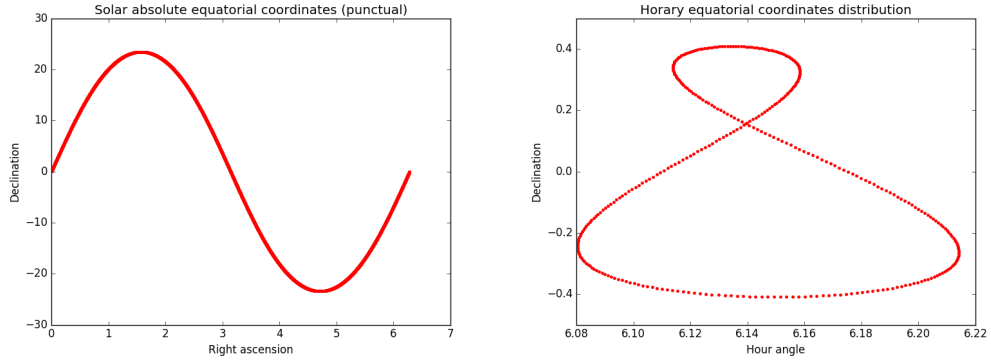

(a) Solar trajectory during one year in absolute equatorial coordinates

(b) Sun's analemma in horary equatorial coordinates

Figure 11: Sun's trajectory in different coordinate systems

4 Data analisys

Now we have our data in a useful coordinate system, we can start with the data analysis. We will do a couple of different studies, done both with a similar data treatment.

4.1 Data sample

The data of the detector have been grouped in 40 angular cells defined by 8 equal intervals of the azimuth angle (ϕ), between -180^o and 180^o, and 5 intervals of the zenith angle (z), between 0^o to 50^o. All the events have been grouped in 10 minutes bins, measuring the frequency of reception of cosmic rays in each cell.

After obtaining the number of cosmic rays received in each cell, we can compute the data using the Python program to obtain this data in the other coordinate systems with the transformations explained at the secction 3.1.

4.2 Acceptance corrections

In order to make correctly this analysis we must take into account the acceptance of the detector. There are two types of acceptances that we have to correct before doing the data analysis. The first one is tha sidereal acceptance. This correction appears because of the fact that the detector covers certain areas of the sky more than others, what causes more cosmic rays detected in some parts of the sky. Knowing which parts of the sky are seen more times by the detector allows us to obtain the correction factor that gives us the number of cosmic rays if all the sky was seen the same number of times.

To obtain the sidereal acceptance, instead of generating all the cosmic rays received, we will consider only one event in each angular interval during a certain period of time. After using the coordinate transformations on this data we will know which parts of the sky are seen more times by the detector, and if we normalize this number of times to 1 on every interval, we obtain the correction factor in each zone.

The other correction we must consider is the angular acceptance. Due to the geometry of the detector, some angles have a bigger acceptance than others, cosmic rays that reach the detector in a perpendicular direction to the planes are detected with more efficiency than those who reach the detector with a certain zenith angle, and the acceptance becomes smaller as the zenith angle increases. By correcting our data with the angular acceptance, all the angles will have the same efficiency.

Figure 12 shows an example of the data before and after the corrections of both acceptances. As we expect from an ideal detector, there is no privileged direction or angle, so after the corrections we have a uniform distribution. The slightly darker stripe appears because we are taking as first approximation that the cosmic ray distribution has to be uniform with $cos(z)$. Actually, this is not the most precise approximation, because cosmic ray distribution is explained better as a uniform distribution in $cos^{\alpha}(z)$, where the α coefficient has an approximate value of $1.8 \sim 1.9$. The first approximation es good enough for our studies of the Sun, because we are going to focus on the region around the coordinate origin.

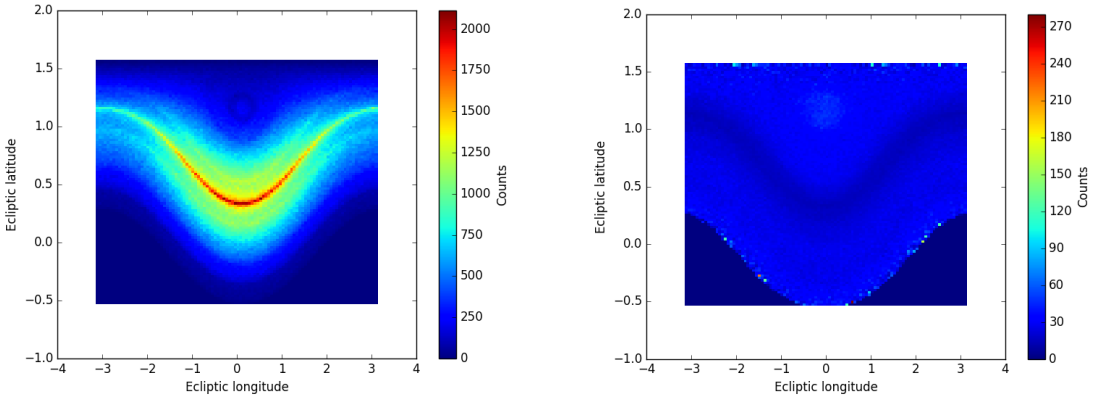

(a) Events registered during one day without corrections

(b) Cosmic ray distribution after doing all the acceptance corrections

Figure 12: Cosmic ray distribution before and after applying the corrections by acceptance

Once we have both acceptances corrected, we have our data as if it has been taken with an ideal detector, with no privileged angles and seeing the sky isotropically.

4.3 Shadow of the Sun

The cosmic ray Sun shadow, as we explained before, can be observed despite the Earth magnetic field, that deflects low energy cosmic rays coming from the Sun, causing a minimum in that direction. The aparent angular size of the Sun is aproximately 0.5^{o}. Studying the size of the shadow we could estimate the angular resolution of the detector. We are going to use data for three different multiplicities, M1, M2 and M3. Multiplicity 1 (M1) corresponds to the lowest energetic rays, so we don't expect to observe the shadow of the Sun, thus, we will not use them in this part of the analysis. M2 and M3 data correspond to more energetic cosmic rays, less affected by magnetic field, and we will try to study the shadow of the Sun with them.

We can study the shadow of the Sun in two different ways. The first one is the geometric shadow of the Sun, generarted by the deflection of the low energetic cosmic rays by the magnetic

field. The best period of time to do this study is around the summer solstice, so we will take the data of two weeks before and two weeks after 21st of June 2015. After applying the corrections by acceptance, if we represent the data during one month, we obtain figure 13. We will start studying the M2 data.

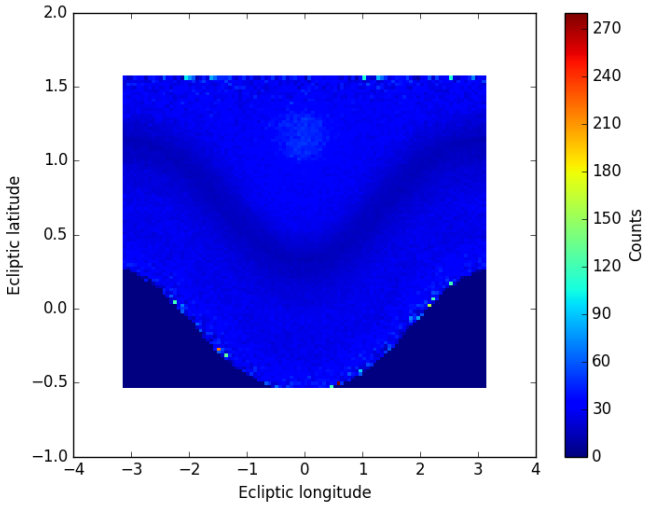

Figure 13: Rate of detected events by TRAGALDABAS between days 157 and 187 (June 6th and July 6th) corrected by acceptance

Now, to study the Sun, we are interested in the part of the plot around the coordinate origin, so expanding that zone, adjusting the scale and the granularity of the figure, we obtain the figure 14.a.

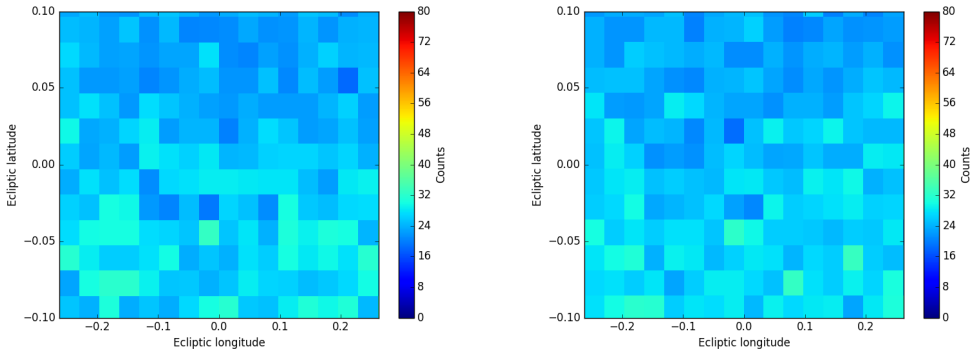

(a) Density plot for M2 expanding the zone around the Sun

(b) Density plot for M3 expanding the zone around the Sun

Figure 14: Rate of M2 and M3 detected events by TRAGALDABAS between days 157 and 187 (June 6th and July 6th). The Sun is at the position (0,0).

Even though the results after applying the corrections by acceptance seemed good, once we amplify the region of the Sun, we are not able to see the structure we expected of the cosmic ray shadow. This is because the detector's angular resolution is not good enough to see that very small structure of 0.5^o (~ 0.01 rad). If we do the same figure for M3, as it happend with M2 data, we won't see the shadow's structure due to the angular resolution as we can see at figure 14.b.

To finish with the analysis of the geometric shadow of the Sun, we can represent also our data in absolute equatorial coordinates. To do this figure we have to take into account the movement of the Sun during the day, so to center the Sun at the coordinate origin, we will represent in both axes the difference between the coordinate of the registered event and the coordinate of the Sun.

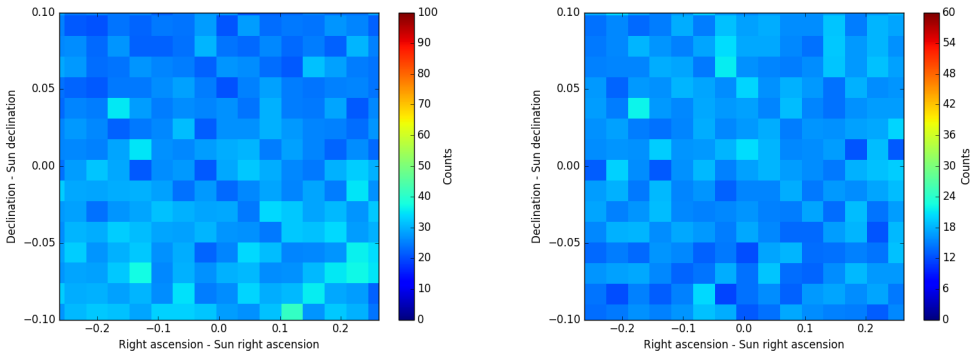

(a) Density plot for M2 data

(b) Density plot for M3 data

Figure 15: Rate of M2 and M3 detected events by TRAGALDABAS between days 157 and 187 (June 6th and July 6th) amplified around the Sun's position in absolute equatorial coordinates

In this case we see that again the distribution is approximately uniform. This is because the angular resolution of the detector, as we said before, that is not good enough to distinguish the structure of the shadow of the Sun.

The second way to study the shadow of the Sun is analyzing the magnetic shadow of the Sun, this is, the variation of the shadow due to changes in the intensity of the Sun's magnetic field. To do this, we will look at the differences between consecutive days. If there is a variation on the magnetic field, it should be reflected on the figures as a variation between two consecutive days. This plots are represented at figure 16.

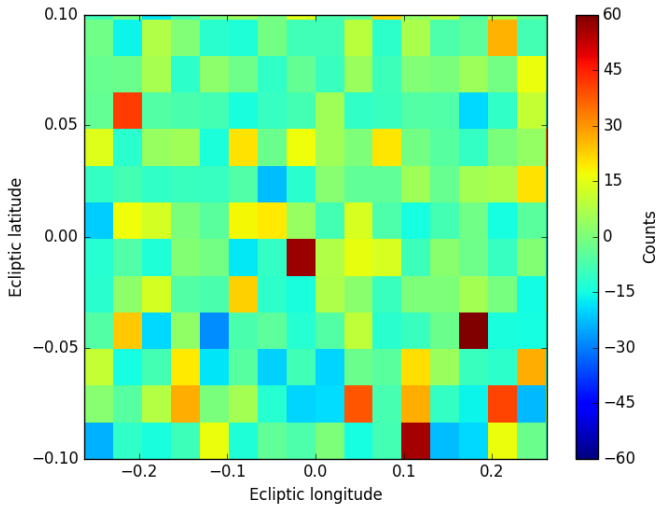

Figure 16: Difference between June 23rd and June 22nd for M1

Again, as we did with the geometric shadow, we are representing only the data for M2

and M3, because we don't expect to observe this phenomenon with the low energy cosmic rays. We used the data during one month around June 21st. As it happened with the geometric shadow, we can see at figure 16 that there are no big variations between consecutive days in the number of events. This could be because there are no big variations on the magnetic field, but probably it is because the detector has not enough angular resolution.

4.4 Forbush Decrease

As we said earlier, we can study also other effects related with cosmic rays in a similar way, like the Forbush Decrease. This effect consists in a rapid decrease of the cosmic ray flux after a coronal mass ejection, due to the magnetic field of the solar wind, that deflects the cosmic rays and preventing them reach the Earth. This effect was produced on June 22nd, 2015, and it was observed by TRGALDABAS.

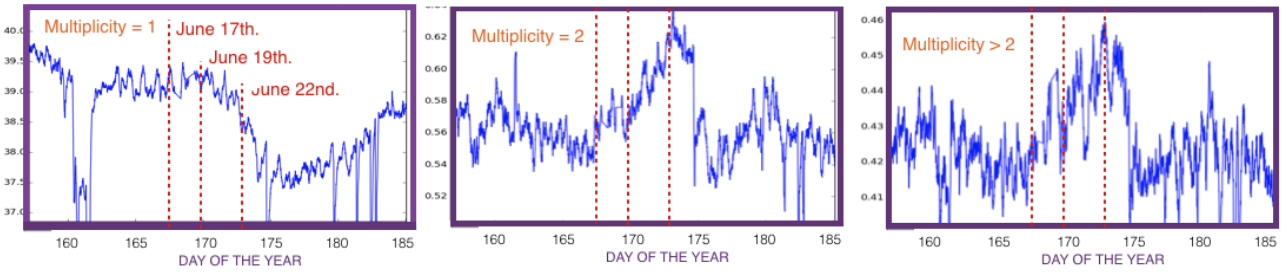

Figure 17: Forbush Decrease detected by the TRAGALDABAS for three different multiplicities

A good way to study the Forbush Decrease is taking the average of three days in which the cosmic ray flux is still normal, like 13, 14 and 15 of June, and see the differences during a month aproximately, from June 13th to July 5th. During the days in which the Forbush Decrease is produced we expect to see a minimum in the cosmic ray flux. It is useful also to see the differences and quotients between consecutive days, so we will observe the evolution of the cosmic ray flux. A good way to represent also this figures is in terms of the number of their standard deviation. We may assume that cosmic rays counting follows Poisson's statistic. If N is the number of events, the standart deviation is:

$$\sigma(N) = \sqrt{N} \tag{16}$$

So the number of standard deviations for differences an quotients, if we call $r = N_2/N_1$, are given by Eq.17 and Eq.18:

$$n_d(\Delta N) = \frac{N_2 - N_1}{\sigma(N_2 - N_1)} = \frac{N_2 - N_1}{\sqrt{\sigma(N_2)^2 + \sigma(N_1)^2}} = \frac{N_2 - N_1}{\sqrt{N_1 + N_2}} \tag{17}$$

$$n_r(r) = \frac{r}{\sigma(r)} = \frac{1}{\sqrt{\frac{1}{N_1} + \frac{1}{N_2}}} = \sqrt{\frac{N_2}{1 + \frac{N_2}{N_1}}} \tag{18}$$

We did this analysis with the M1 data, obtaining the results shown at figure 18.

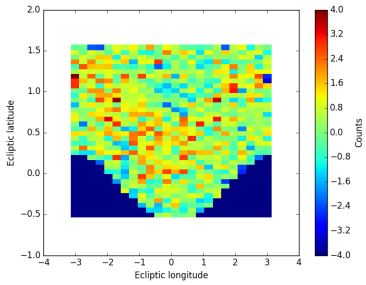

(a) Density plot for day 172 (June 21st)

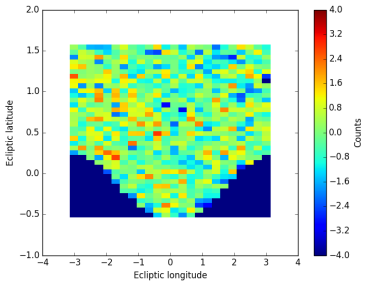

(b) Density plot for day 173 (June 22nd)

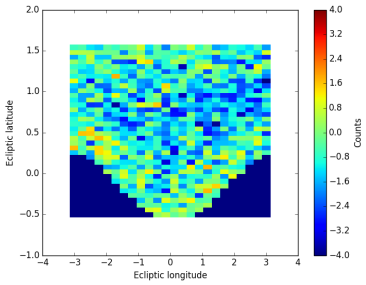

(c) Density plot for day 174 (June 23rd)

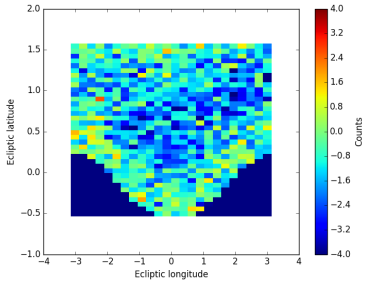

(d) Density plot for day 175 (June 24th)

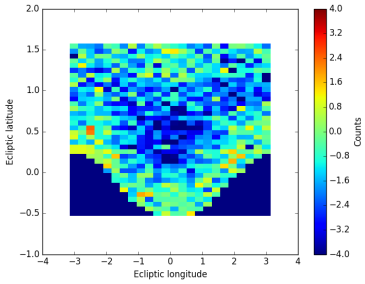

(e) Density plot for day 176 (June 25th)

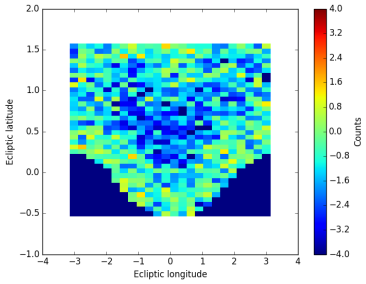

(f) Density plot for day 177 (June 26th)

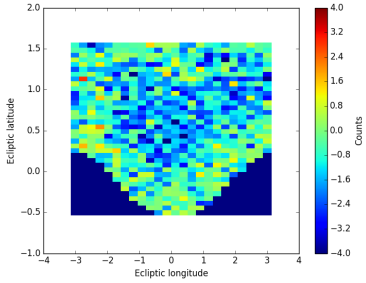

(g) Density plot for day 178 (June 27th)

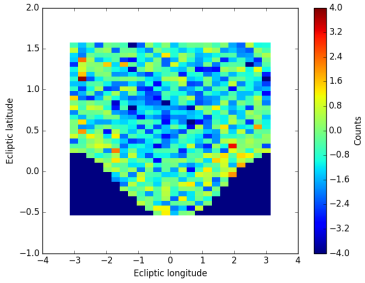

(h) Density plot for day 179 (June 28th)

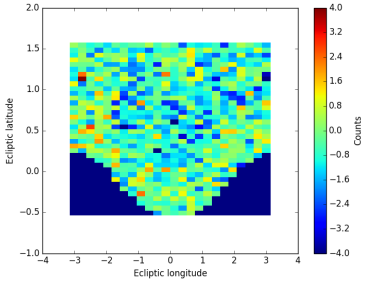

(i) Density plot for day 180 (June 29th)

Figure 18: Density plots for M1 data with a granularity of 24x36. Figures corresponding to the ratio between the average of days 164, 165 and 166 (June 13th, 14th and 15th) and the selected day.

As we expected, during the Forbush Decrease (June 22nd), we can see a rapid decrease of the number of registered events, perfectly shown at figure 18, where we can observe that after days 172 and 173, there is a big decrease at the day 174. At days 179 and 180 the number of detected cosmic rays starts to come back to normal, as we can see at 18.h and 18.i.

This plots are representing the ratio between the average of three days and a the selected day during the Forbush Decrease. If we represent the same figures, but instead of making the ratios we plot the differences, we will obtain practically the same figures. This can be explain using Eq.17 and Eq.18. When $N_1 \simeq N_2$, both expressions can be approximated by Eq.19.

$$n_r \simeq \frac{N_2 - N_1}{\sqrt{N_1 + N_2}} = n_d \tag{19}$$

It is important to highlight that during some of the studied days, there was an error with the data acquisition, as we show at figure 19.

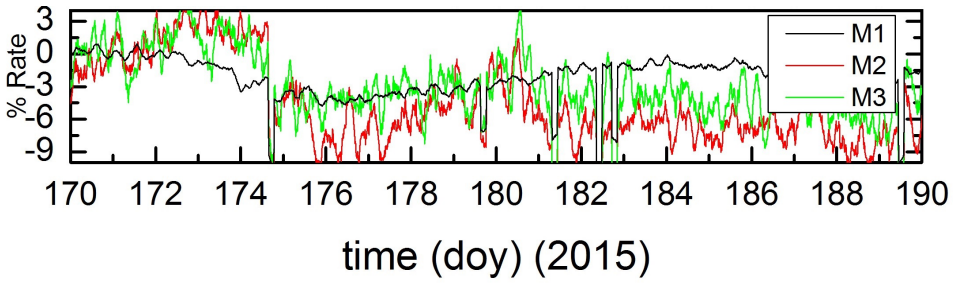

Figure 19: Rate of detected events by TRAGALDABAS between days 170 and 190. Unexpected sharp minima may be observed at days 174, 179, 181 and 182.

Observing this figure, we notice a sudden decrease of the number of events at days 174, 179, 181 and 182. This was because an error in the detector's system, and is not related with de Forbush Decrease. This was corrected interpolating the data of the day before and the day after this error. The correction is shown at figure 20, where we can see a big blue spot due to this error. After the correction we managed to normalize the behavior of the detector.

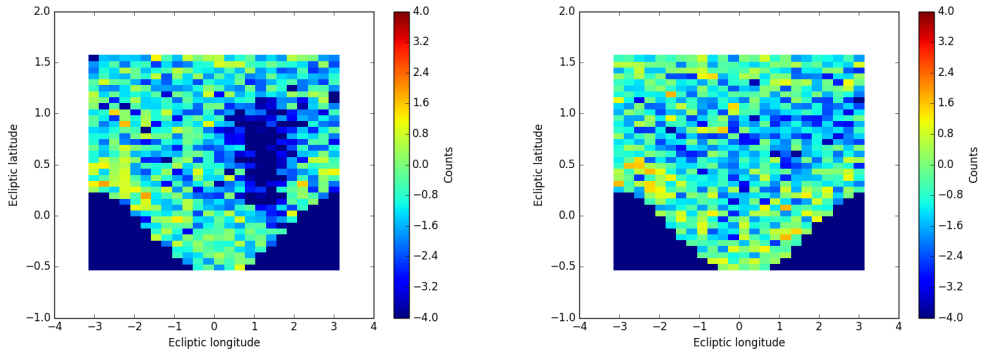

(a) Density plot before the correction

(b) Density plot after the correction

Figure 20: Density plots before and after the corrections because of the error suffered by the detector

We can do the same analysis for M2 and M3 data, representing again the ratios (or the differences) between one day and the average of five days. In this case we are taking as reference five days instead of three because the number of events for M2 and M3 is smaller. Then, representing for M2 the same days that we did for M1, we obtain the results shown at the figure 21. We are only representing the M2 data because the results that we are going to obtain are basically the same.

As we can appreciate observing this plots, the results are not what we expected. During the Forbush Decrease we expect to observe a minimum in the cosmic ray flux because of the deflection caused by the magnetic field during the coronal mass ejection, but instead of

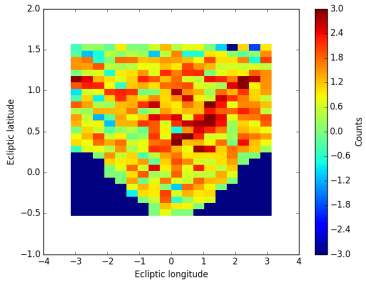

(a) Density plot for day 170 (June 19th)

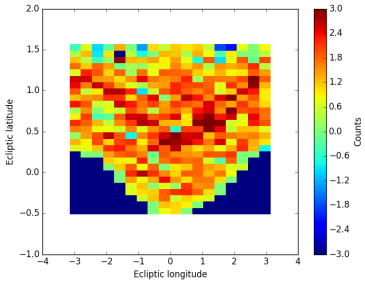

(b) Density plot for day 171 (June 20th)

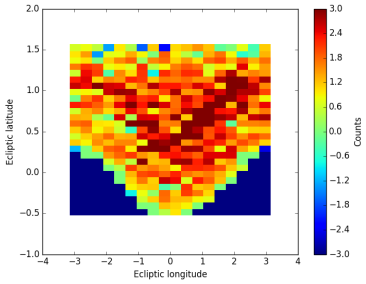

(c) Density plot for day 172 (June 21st)

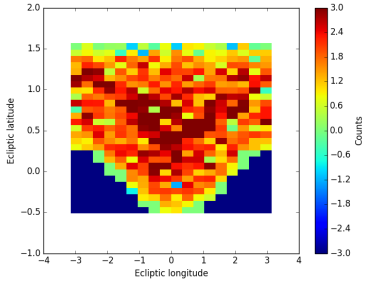

(d) Density plot for day 173 (June 22nd)

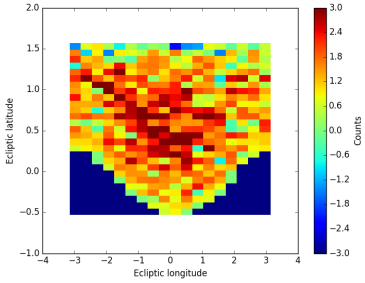

(e) Density plot for day 174 (June 23rd)

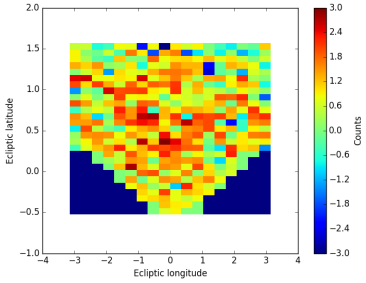

(f) Density plot for day 175 (June 24th)

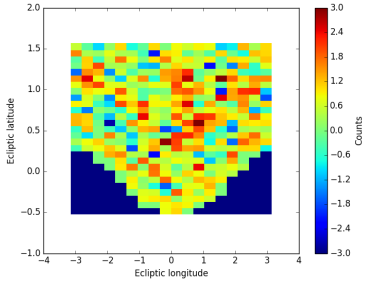

(g) Density plot for day 176 (June 25th)

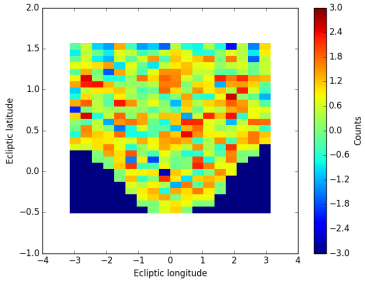

(h) Density plot for day 177 (June 26th)

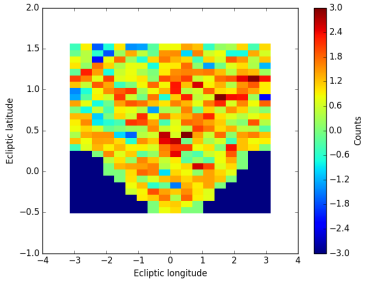

(i) Density plot for day 178 (June 27th)

Figure 21: Density plots for M2 data with a granularity of 18x27. Figures corresponding to the ratio between the average of days 162, 163, 164, 165 and 166 (June 11th, 12th, 13th, 14th and 15th) and the selected day.

that, we see that, for M2 and M3, the data shows a big maximum untill day 176 (June 25th) aproximately, where the flux starts to come back to normal.

This effect is still an unknown and it should be studied more deeply for full understanding.

To conclude the study of the Forbush Decrease, a usefull analysis is to estimate the size of the cloud of coronal mass ejected by the Sun and its position during the days in which the Forbush Decrese occurs. This allows us to make aproximation of how big the decrease was and locate the most affected regions of the sky.

In order to do this, we obtained the minimum value of the figures for M1 and the maximum value for M2 and M3 and their positions during a 10 day period (from June 20th to

June 30th). Also we obtain the number of points with a value grater than the 20% of the value of the absolute minimum of those 10 days for M1 (and with a value less than the 20% of the value of the maximum for M2 and M3), to estimate the size of the cloud, assuming that the points with a value close to the minimum (or maximum) are concentrated around it, forming the cloud.

After doing this analysis for M1 data, we obtain the values shown at the table 1. The values of the coordinates are taking according to the position in the data matrix. With that position we can estimate the location of this minimum in the sky.

Day of year	Depth	Minimum position	N
June 20th (Day 171)	-3.57	(73,43)	2490
June 21st (Day 172)	-4.07	(78,31)	2523
June 22nd (Day 173)	-5.04	(62,51)	2721
June 23rd (Day 174)	-6.37	(62,50)	3462
June 24th (Day 175)	-4.62	(62,48)	3321
June 25th (Day 176)	-4.18	(62,48)	3426
June 26th (Day 177)	-4.19	(16,58)	3429
June 27th (Day 178)	-4.10	(62,53)	3182
June 28th (Day 179)	-5.22	(36,13)	3108
June 29th (Day 180)	-3.82	(62,52)	2926
June 30th (Day 181)	-5.29	(25,95)	2917

Table 1: M1 data to estimate the size (N) of the coronal mass cloud and the relevance of the Forbush Decrease during 10 days

N represents the number of points with a value lower than the 20% of the absolute minimum. As we expected, during the Forbush Decrease, the number of points with values close to the value of the absolute minimum are higher. Looking at the value of N we can also estimate the days when the Forbush Decrease has more importance, i.e., from June 23rd to June 26th. This is consistent with the plots represented at figure 18, where we had a big minimum during those days, and from June 27th, the flux starts to increase up to the normal values. A big value of N also represents that the size of the cloud increases, so during those four days, the cloud becomes bigger and minimizes the cosmic ray flux.

From the data value of the position in the data matrix we can obtain that, during the Forbush Decrease, the cloud stays approximately in the middle part of the figure 18, as we expected observing these plots.

Finally, doing the same analysis for M2 (for M3 we will get very similar results to M2), we obtain the values at table 2.

In this case, N represents the number of points with a value higher than the 20% of the value of the absolute maximum. Again, observing the values of the maximum of each day and the values of N, we see that this is consistent with the figure 21 obtained before, where we saw a big increase starting at June 20th, reaching a big maximum around the days 21st or 22nd, and then decreasing to the normal values during the following days. With this data, we conclude, as we did with M1 values, that the cloud becomes bigger between June 22nd and June 26th, when the data differs more from the normal values.

Day of year	Height	Maximum position	N
June 20th (Day 171)	3.92	(56,71)	5348
June 21st (Day 172)	3.77	(78,31)	5545
June 22nd (Day 173)	4.02	(45,47)	5676
June 23rd (Day 174)	3.89	(62,50)	5388
June 24th (Day 175)	3.58	(62,48)	5039
June 25th (Day 176)	3.46	(55,56)	4823
June 26th (Day 177)	3.41	(31,62)	4821
June 27th (Day 178)	3.36	(53,25)	5012
June 28th (Day 179)	3.44	(10,66)	5078
June 29th (Day 180)	3.53	(19,77)	5322
June 30th (Day 181)	3.67	(20,66)	5250

Table 2: M2 data to estimate the size (N) of the coronal mass cloud and the relevance of the Forbush Decrease during 10 days

Also notice that with the position of the maximum we can deduct that the cloud stays around the middle of the figures during the days when the Forbush Decrease is more important, but in this case we have more statistic fluctuations because we have a number of data much less than for M1, so we can estimate the position with the same precision.

5 Conclusions

In this work we have taken the first step of the study of the angular resolution of the detector and the shadow of the Sun. Unfortunately, the current resolution of the detector is still not good enough to distinguish the shadow, but it was important to begin this analysis to apply it in the future, when the detector reaches better angular resolution. This analysis could be complemented at later projects with the study of the shadow of the Moon.

The analysis and corrections of the angular and the sidereal acceptances has already been made, which will facilitate future studies.

At the moment, the TRAGALDABAS is being improved with the development of a better tracking system with better angular precision. So, in a near future, this analysis could be repeated with more accurate data.

We have analyzed the data during the Forbush Decrease observed at June 22nd. The detector was able to observe this phenomenon with precision. Despite there were a couple of errors with the data acquisition system, we were able to corrected those errors and made a statistic analysis of the data for three different multiplicities, low (M1), medium (M2) and high (M3).

We have analized the size and evolution of several effects observed with different multiplicities.

References

[1] A. Morozova, P. Ribeiro, and Tragaldabas Collaboration Team, "Cosmic rays flux and geomagnetic field variations at midlatitudes," in *EGU General Assembly Conference Abstracts*, vol. 16 of *EGU General Assembly Conference Abstracts*, p. 7516, May 2014.

[2] H. Alvarez-Pol, A. Blanco, J. J. Blanco, J. Collazo, P. Fonte, J. A. Garzón, A. Gómez, G. Kornakov, T. Kurtukian, L. Lopes, M. Morales, A. Morozova, M. A. Pais, M. Palka, V. Pérez Muñuzuri, P. Rey, P. Ribeiro, M. Seco, and J. Taboada, "TRAGALDABAS: A new high resolution detector for the regular study of cosmic rays," *Journal of Physics Conference Series*, vol. 632, p. 012010, Aug. 2015.

[3] A. Blanco, J. Blanco, J. Collazo, P. Fonte, J. Garzón, A. Gómez, G. Kornakov, T. Kurtukian, A. L. Agüera, J. López, *et al.*, "TRAGALDABAS: a new RPC based detector for the regular study of cosmic rays," *Journal of Instrumentation*, vol. 9, no. 09, p. C09027, 2014.

[4] I. I. Yashin, I. Astapov, N. Barbashina, A. Dmitriyeva, A. Petrukhin, and V. Shutenko, "URAGAN & TRAGALDABAS: two complementary approaches for the regular survey of cosmic rays,"

[5] J. A. Garzón, "TRAGALDABAS: a high performance detector for the regular study of cosmic ray properties,"

[6] X. Xu, M. Collaboration, *et al.*, "The Cosmic Ray Shadows of the Moon and the Sun Detected by the Milagro Gamma Ray Observatory," in *International Cosmic Ray Conference*, vol. 7, p. 4065, 2003.

[7] I. Reda and A. Andreas, "Solar position algorithm for solar radiation applications," *Solar energy*, vol. 76, no. 5, pp. 577–589, 2004.

[8] G. E. Christopher, *Physics from the Very-High Energy Cosmic-Ray Shadows of the Moon and Sun with Milagro*. PhD thesis, New York University, 2011.

[9] Z. FENGRONG, "Correlation between Solar Activity and the Cosmic Ray Sun Shadows observed with the ARGO-YBJ experiment,"

[10] M. Amenomori, S. Ayabe, L. Ding, Z. Feng, Y. Fu, H. Guo, M. He, K. Hibino, N. Hotta, Q. Huang, *et al.*, "A study of the shadowing of galactic cosmic rays by the sun in a quiet phase of solar activity with the Tibet air shower array," *The Astrophysical Journal*, vol. 541, no. 2, p. 1051, 2000.

[11] O. Enriquez, A. Lara, *et al.*, "The Galactic cosmic-ray Sun shadow observed by HAWC," *arXiv preprint arXiv:1508.07351*, 2015.

[12] "Capítulo 5: Coordenadas celestes," *Universidad de Bogotá*.

[13] "Capítulo 7: Tiempo en astronomía," *Universidad de Bogotá*.